# Evaluation of blood oxygen saturation *in vivo* from diffuse reflectance spectra

**Alexander A. Stratonnikov**
**Victor B. Loschenov**
General Physics Institute
Laser Biospectroscopy Lab
38, Vavilov Street
Moscow 117942, Russia

**Abstract.** A simple method to evaluate the hemoglobin oxygen saturation and relative hemoglobin concentration in a tissue from diffuse reflectance spectra in the visible wavelength range is put forward in this paper. It was assumed that while oxygenated and deoxygenated hemoglobin contributions to light attenuation are strongly variable functions of wavelength, all other contributions to the attenuation including scattering are smooth wavelength functions and can be approximated by Taylor series expansion. Based on this assumption, a simple, robust algorithm suitable for real time monitoring of the hemoglobin oxygen saturation in the tissue has been derived. This algorithm can be used with different fiber probe configurations for delivering and collecting light passed through the tissue. An experimental technique using this algorithm has been developed for *in vivo* monitoring during artery occlusion and *in vitro* monitoring of blood samples. The experimental results obtained are presented in the paper. © *2001 Society of Photo-Optical Instrumentation Engineers.*
[DOI: 10.1117/1.1411979]

Keywords: tissue spectroscopy; blood oxygenation; tissue absorption; diffuse reflectance.

## 1 Introduction

There are many approaches to evaluate the blood oxygen saturation *in vivo* from tissue diffuse reflectance spectra.[1–22] Hemoglobin contained in erythrocytes is the main tissue absorber in the visible and very near infrared range. As a hemoglobin absorption spectrum is different for oxygenated and deoxygenated forms[18,23] (by this reason the blood in an artery and a vein varies in color), this fact can be used for quantification of the blood oxygen saturation in the tissue *in vivo*. The central problem with the evaluation of blood oxygen saturation for the tissue *in vivo* is to take into account the influence of the scattering, other tissue absorbers and heterogeneous hemoglobin distribution.

To quantify the relative oxyhemoglobin and deoxyhemoglobin concentrations as well as other tissue absorbers in the tissue using optical spectroscopy, the following two steps are usually performed. First, the total absorption ($\mu_a$) and reduced scattering ($\mu_s'$) tissue coefficients are extracted from the experimental measurements at several wavelengths. For a uniform semi-infinite medium it can be done by time resolved methods in frequency and time domain[10,11,20,24,25] or spatially resolved methods.[17,29,26–30] The number of wavelengths whereby the total absorption coefficient is evaluated should be at least equal to the number of the tissue absorbers contributing to absorption in the spectral range under analysis. If the measurement method gives no way of obtaining absorption and reduced scattering coefficients independently, for example, in steady-state measurements without spatial resolu-

tion absorption and reduced scattering coefficients are coupled to each other, some assumption should be done about behavior of the reduced scattering coefficient or this value requires independent measurements. Using this information and applying some model for diffuse reflection dependence upon tissue optical properties, the absorption coefficient can be extracted from simple steady-state diffuse reflectance measurements.[31] On evaluating the total tissue absorption coefficient at several wavelengths, the concentrations of individual absorbers may be obtained as it is done in the usual spectroscopy problem of multicomponent systems. If the absorption spectra of all the species contributing to the tissue absorption are known, it is done by solving normal equations with the least square method. The sophisticated chemometrics methods (partial least square, principle component analysis[19] or singular value decomposition[32]) can be also applied if information about absorbing species is not complete.

An original self-consistent approach for evaluation of the blood oxygen saturation and the relative hemoglobin concentration from diffuse reflectance spectrum obtained with fiber probe geometry without spatial resolution is described in this work. The method is applied in the visible wavelength range, where the spectral difference between oxygenated and deoxygenated hemoglobin is rather high. The advantage of the proposed approach is its simplicity and applicability to different fiber probe geometries used to deliver and collect light passed through the tissue. The relation between a diffuse reflectance signal and tissue optical properties in terms of photon path length distribution function is detailed in the next section. The existing theoretical approaches extracting the absorption coef-

Address all correspondence to Dr. Alexander A. Stratonnikov. Tel/Fax: 095-324-6363; E-mail: biospec@online.ru
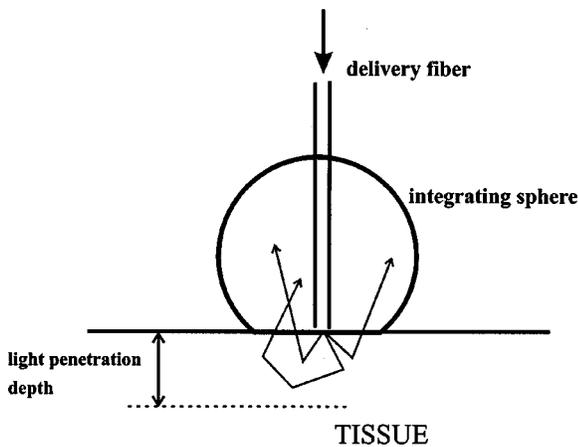
**Fig. 1** Integrating sphere geometry for collecting diffuse reflected photons. The sampling depth for this configuration is determined mainly by the light penetration depth $\delta$.

ficient are briefly reviewed and discussed therein. Taylor expansion method is presented in Sec. 3. In linear approximation it results in an effective algorithm for blood oxygen saturation calculation. An experimental setup for diffuse reflectance and diffuse transmittance measurements is described in Sec. 4. Finally, the experimental results obtained on human skin during artery occlusion and blood samples during photochemical deoxygenation are presented and discussed in Sec. 5.

## 2 Diffuse Reflectance and Photon Path Length Distribution Function

To evaluate the spectral dependencies of absorption and scattering coefficients it is convenient to consider the light attenuation $A(\lambda)$ defined by the following expression:

$$A(\lambda) = -\ln\left(\frac{I}{I_0}\right), \qquad (1)$$

where $I_0$ and $I$ are the total photon flows coming out from the delivery fiber and entering into the receiving fiber correspondingly. In the case of integrating sphere configuration the value $I$ is the integrated photon flow measured by the sphere (see Figures 1 and 2). Sometimes the dependence (1) is called the absorption without correction for the scattering.

Due to the strong tissue scattering the photon path lengths through the tissue contributing the measured signal have a
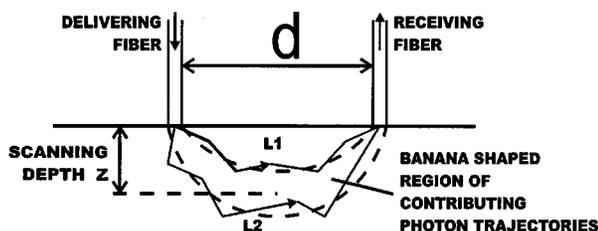


**Fig. 2** Probe arrangement with distantly placed fibers for the measurement of tissue diffuse reflectance spectra *in vivo*. The sampling depth is determined by the light penetration depth $\delta$ and fiber separation distance $d$.

distribution with some probability function $P$. The intensity of a light signal in the receiving fiber or in the integrating sphere is determined by absorbing and scattering properties of the tissue as well as by measurement configuration and may be expressed through the path length probability function by the following relation:

$$I/I_0 = \int_0^\infty P(\mu_s, g, l) \cdot \exp(-\mu_a l) dl, \qquad (2)$$

where $\mu_s$ is the scattering tissue coefficient, $\mu_a$ is the absorption coefficient, $g$ is the scattering anisotropy factor, $l$ is the photon path length through the tissue on the trajectory between the delivering and receiving fibers (see Figure 2), and the dimensionless value $P(\mu_s, g, l) dl$ is the probability that the photon path length will be in the interval $[l, l+dl]$ between the delivering and receiving fibers in the absence of absorption (path length distribution function). The path length distribution function $P$ depends on the scattering tissue properties ($\mu_s$ and $g$) as well as on the geometry of the measurements (fiber probe spatial configuration). The dimension of $P$ function is the inverse dimension of the length. The integral of the distribution function over all photon path lengths (normalization of the path length distribution function) determines the attenuation of photon flux between the delivery and receiving fibers due to the scattering alone. It should be also noted here that integral (2) represents Laplace transform of the path length distribution function $P(l)$.

As mentioned above, the path length distribution function is strongly dependent on the spatial configuration of the fiber probe as its geometry defines the trajectories of photons, which passed through the tissue and reached the detector. Two limiting cases of geometrical configurations for the semi-infinite medium are usually discussed. The first is the integrating sphere arrangement when all light reemitted from the tissue is collected as shown in Figure 1. Practically it may be realized only with the use of an integrating sphere for collecting all the diffuse reflected light. However, the use of the integrating sphere is very inconvenient for *in vivo* measurements. A sampling depth for this configuration is determined mainly by the light penetration depth $\delta$. In the second limiting case the delivery and receiving fibers (or a light emitter and a detector) are placed apart at the distance $d$ which is much greater than the fiber diameter (size of the emitter and the detector) as shown in Figure 2. In this case the photon trajectories through the tissue form a banana shaped region with the ends at the positions of the delivery and receiving fibers. The sampling depth for this configuration is proportional to $\sqrt{2}d/4$ in the weak absorption limit ($d \ll \delta$) and $\sqrt{d\delta/2}$ in the strong absorption limit ($d \gg \delta$).[33,34] Thus, in this case increasing the fiber separation makes it possible to increase the sampling depth. This configuration is applied to cerebral blood oxygen saturation measurements in the near infrared spectral range. Of course, there may be intermediate cases such as closely spaced delivery and receiving fibers which are greater in diameter than the distance between the fibers. Approximate analytical solutions relating tissue optical properties and diffuse reflected signal intensity have been obtained only for these limiting cases of the integrating sphere and the spatially

placed fibers. For intermediate cases one may use a collection efficiency factor scaling the measured signal to these analytical expressions.

In the case of a transparent medium for a configuration when delivering and receiving fibers are placed on opposite sides of a sample with thickness $L$, all the photons have the same path length $L$, and the path length distribution function is reduced to Dirac delta function: $P(l) = \delta(l - L)$. On substituting this function in Eq. (2) it is reduced to the Beer–Lambert law relating signal attenuation in the nonscattering absorbing medium with the absorption coefficient $\mu_a$ and the path length $L$

$$A = -\ln\left(\int_0^\infty \delta(l - L) \cdot \exp(-\mu_a l) dl\right) = \mu_a \cdot L. \quad (3)$$

In the presence of the scattering the relation between the measured signal attenuation and the absorption coefficient is complicated. Accurate approaches for obtaining the absorption and scattering tissue coefficients are based on the time resolved measurements. The time resolved reemittance signal represents in fact the path length distribution function with change of product speed of light in the tissue and time on path length $l$ multiplied by the absorption term $\exp(-\mu_a l)$. An analytical approximation for the path length distribution function (with zero boundary condition) for the fiber configuration shown in Figure 2 has been obtained from the diffusion theory[24]

$$P(l) \cdot \exp(-\mu_a l) = z_0 (4\pi D)^{-3/2} l^{-5/2}$$
$$\times \exp\left(-\frac{d^2 + z_0^2}{4Dl}\right) \cdot \exp(-\mu_a l) \cdot ds, \quad (4)$$

where $z_0 = 1/\mu_s'$, $\mu_s' = \mu_s(1 - g)$, $D = 1/3\mu_s'$, $d$ is distance between the source and the detector, $ds$ is the cross-sectional area of the receiving fiber. Fitting the experimental time resolved reemitted signal with function (4) (or more sophisticated one taking into account different boundary conditions[25,35]) one can get the values of $\mu_a$ and $\mu_s'$.[24] But this method requires a complicated technique for its realization and makes application in clinical conditions difficult.

The steady-state experimental methods are easier to apply in practice. In diffuse approximation the formula relating the intensity of the steady-state measured signal with tissue optical properties and the fiber separation distance can be obtained directly from Eq. (2). Substituting relation (4) for the path length distribution function into Eq. (2) and calculating the resulting integral we obtain the following relation for the steady-state case in the diffusion approximation:

$$I/I_0 = \int_0^\infty P(l) \cdot \exp(-\mu_a l) dl$$
$$= \frac{1}{2\pi\mu_s'} \cdot \left(\frac{1}{\delta} + \frac{1}{d}\right) \cdot \frac{1}{d^2} \cdot \exp(-d/\delta) \cdot ds, \quad (5)$$

$$\delta = 1/\sqrt{3\mu_a(\mu_a + \mu_s')} \approx 1/\sqrt{3\mu_a\mu_s'}.$$

Measuring the reemitted signal at different distances $d$ between delivery and receiving fibers and fitting this dependence by relation (5) (or more sophisticated one taking accurately into account the influence of the boundary[25,26]), it is possible to get the values of $\mu_a$ and $\mu_s'$. In Ref. 19 this technique was applied to the evaluation of the blood oxygen saturation in the near-infrared (NIR) spectral range by fitting the obtained wavelength dependence of tissue absorption coefficient with the spectra of oxygenated and deoxygenated hemoglobin as well as background absorption.

In the following consideration we will be restricted to the case when we measure the reemitted signal without spatial resolution. In this case it is not possible to get the values of absorption and scattering coefficients independently. Nevertheless, assuming the wavelength dependence of scattering and knowing the absorption spectra of the species present in the tissue, it is possible to evaluate concentrations of the tissue absorbers. However, the use of Eq. (5) for this purpose is restricted only to the diffuse approximation region and the spatially separated fiber probe configuration (Figure 2). For example, when we use a probe arrangement with closely spaced fibers the signal dependence is rather described by that obtained for integrating sphere configuration.

For the integrating sphere configuration there are two simple relations between the measured reflected signal and the tissue properties. One is based on Kubelka–Munk theory for light transport in tissue,[9] and another has been obtained by fitting Monte Carlo results with the analytical expression.[31] According to the Kubelka–Munk theory the diffuse reflectance coefficient $R_d$ is described as follows:

$$R_d = I/I_0 = \exp(-A) = 1 - \frac{K}{S}\left(\sqrt{1 + 2\frac{S}{K}} - 1\right), \quad (6)$$

where $K$ and $S$ are absorption and scattering Kubelka–Munk coefficients, respectively. The Kubelka–Munk absorption coefficient $K$ can be related to the tissue absorption coefficient $\mu_a$. In Ref. 9 this approach was used to evaluate the blood oxygen saturation by modeling tissue absorption as a sum of oxygenated and deoxygenated hemoglobin and approximating the Kubelka–Munk scattering coefficient by a smooth wavelength function. Actually, this approach is very close to ours given bellow. The difference is that we are not restricted to the particular fiber probe geometry and derive the results starting from the exact relation (2) for the diffuse reflectance (or transmittance) signal expanding it in Taylor series and omitting higher orders (see below).

Another relation for the integrating sphere configuration was obtained by Jacques[31] and tested using Monte Carlo technique. According to it the expression for diffuse reflectance coefficient can be written as

$$R_d \approx \exp(-7.8 \cdot \mu_a \cdot \delta), \quad (7)$$

where $\delta$ is the light penetration depth defined in Eq. (5). This relation was used in Ref. 31 to evaluate bilirubin content in skin. Relation (7) clearly demonstrates that the mean photon path length through the tissue in the integrating sphere configuration can be approximated by $7.8\delta$. Relations (6) and (7) are valid only for the integrating sphere configuration (i.e., when all the light diffusely reflected from the tissue is col-

lected). Fiber probes collect actually only a part of the reflected signal. This should be taken into account by a collection efficiency factor[31] when applying these relations to data interpretation. It should be noted also that when relations (5)–(7) are applied to evaluate the concentrations of absorbing species in the tissue one must know the wavelength dependence of the scattering coefficient. This information may be obtained from experimental data or modeled. For example, it was shown in Refs. 14 and 36 that for the visible and NIR range the wavelength dependence of the scattering coefficient can be approximated by: $\mu_s' \sim 1/\lambda^{0.37}$, although the Rayleigh contribution, which is proportional to $1/\lambda^4$, may also be substantial for short wavelengths.

A very important question, which we have not touched so far, concerns the heterogeneous distribution of the tissue absorbers. Hemoglobin is located in vessels, which form a complex tangled network inside the tissue, while melanin is concentrated in a thin superficial epidermis layer. These nonuniformities result to distortion of diffuse reflectance spectra as compared to that predicted from the models previously described. The heterogeneous distribution of melanin in the tissue and its influence on the diffuse reflectance spectra were considered in Ref. 31.

## 3 Tayor Series Expansion Model

Our approach given below is based on the assumption that attenuation $A$ is a smooth (analytical) function of $\mu_a$ and the changes of $\mu_a$ over the spectral range under analysis are not high. We start from the exact relation for $A$ based on Eq. (2) and approximate the attenuation by Taylor series expansion at some value $\mu_a = \mu_a^0$ as follows:

$$A = -\ln(I/I_0)$$
$$\approx A(\mu_a^0) + A'(\mu_a - \mu_a^0) + \frac{A''}{2!}(\mu_a - \mu_a^0)^2 + \dots \quad (8)$$

The value of $\mu_a^0$ will be determined in a self-consistent way to minimize difference between experimental and modeled data. Intuition suggests that this value lies in the middle of $\mu_a$ variance interval in the spectral range under analysis. For the following analysis (linear approximation) we save only two terms (constant and linear) in expansion (8). It should be emphasized that Taylor coefficients are functions of wavelength through the dependence of $\mu_s(\lambda)$ but do not depend on $\mu_a$. It is also possible to allow for the quadratic term in Eq. (8) resulting in a more complicated model with the greater number of fitted parameters. Such a model may occur to be useful for analysis of data acquired with a high signal to noise ratio or for high changes in the absorption coefficient through the analyzed spectral range. For the data obtained in our experimental setup, the linear approximation gives the required accuracy. The applicability of linear approximation [smallness of the quadratic term in Eq. (8)] can be expressed in the following form:

$$\frac{1}{2}|A''| \cdot \Delta\mu_a \ll A', \quad (9)$$

where $\Delta\mu_a$ is the variance of the tissue absorption coefficient in the spectral range under investigation.

The expansion coefficient $A'$ (before a linear term) has the sense of the average photon path length through the tissue $\langle L \rangle$. It easily can be observed by calculating the derivative of $A$ over $\mu_a$ from Eq. (2)

$$\langle L \rangle = \left. \frac{\partial A}{\partial \mu_a} \right|_{\mu_a = \mu_a^0} = \frac{\int_0^\infty l \cdot P(\mu_s, g, l) \cdot \exp(-\mu_a^0 l) dl}{\int_0^\infty P(\mu_s, g, l) \cdot \exp(-\mu_a^0 l) dl}. \quad (10)$$

It is clear from this relation that the $\langle L \rangle$ is the averaged photon path length through the tissue for the distribution function $P(\mu_s, g, l)\exp(-\mu_a l)$. The angle brackets denote further the averaging with the distribution function given above. It should be noted that with the use of $\langle L \rangle$ from Eq. (10) relation (8) in the linear approximation is similar to the modified Beer–Lambert law

$$A = A_0 + \langle L \rangle \cdot \mu_a, \quad (11)$$

which is applied for evaluating the changes in $\mu_a$ and calculating the relative concentrations of oxygenated and deoxygenated cerebral hemoglobin from the NIR spectral range. The difference here is that in our approach we consider $\langle L \rangle$ as a Taylor coefficient which is not dependent on $\mu_a$, and the following correction is not intended to model the dependence of $\langle L \rangle$ from $\mu_a$ as it is done in the modified Beer–Lambert law but to take into account the next (quadratic) term in Taylor series expansion (8). The unknown contribution of scattering $A_0$ in the modified Beer–Lambert law is compensated by analyzing the changes in attenuation $\Delta A$ over time relative to an arbitrary initial moment so that one could get the corresponding changes in time of the absorption coefficient $\Delta\mu_a$. In our approach we analyze the spectral dependence of complete attenuation $A$ (to within a constant wavelength term), and the absolute blood oxygen saturation may by extracted from a single spectral curve.

It can also be shown that the second derivative of attenuation over $\mu_a$ can be expressed as

$$A'' = -(\langle L^2 \rangle - \langle L \rangle^2) = -\langle (L - \langle L \rangle)^2 \rangle. \quad (12)$$

Thus, it can be said that application of Taylor series expansion means the approximation of the path length distribution function by its moments. The first moment is a mean value and the second moment is a dispersion of a random variable. The condition for applicability of the linear approximation (9) with allowance for Eq. (12) takes the form

$$(\langle L^2 \rangle - \langle L \rangle^2) \cdot \Delta\mu_a \ll \langle L \rangle. \quad (13)$$

Intuition suggests that the applicability of the liner approximation is restricted by the region, where the changes of absorption coefficient $\Delta\mu_a$ are small as compared to the averaged value $\mu_a^0$. It is also clear that this criterion is dependent on the path length distribution function, the narrower distribution function the more favorable this criterion. In the limiting case of a super narrow path length distribution function which may be approximated by Dirak delta function $P(l) = \delta(l - L)$ the conditions of the criterion (13) will be adequate everywhere as its left side equals to zero. If we take a more realistic case of the path length distribution function with narrow but finite dispersion $\Delta L$ approximated by Gaussian distri-

bution $P(l) = \exp\{-[(l-\langle L\rangle)/2\Delta L]^2\}/\Delta L(2\pi)^{1/2}$ so that $(\Delta L/\langle L\rangle) \ll 1$, the criterion (13) is reduced to the following relation:

$$(\Delta\mu_a \cdot \langle L\rangle) \cdot \left(\frac{\Delta L}{\langle L\rangle}\right)^2 \ll 1. \tag{14a}$$

The dimensionless term $\Delta\mu_a\langle L\rangle$ has the sense of attenuation changes in the spectral range under analysis. This value typically is less or of the order of unity. For example, the estimation of attenuation changes in human skin *in vivo* in the visible range for our fiber probe geometry (see Figure 4) gives the value of $\Delta\mu_a\langle L\rangle$ in the range between 0.4 and 1. Analyzing relation (14a) one can conclude that for narrow path length distribution functions $((\Delta L/\langle L\rangle) \ll 1)$ the applicability of the linear approximation is rather favorable and may extend even beyond the small variances in the absorption coefficient. In the opposite case of a broad path length distribution function the condition (13) will not be so favorable. For example, just to evaluate the most unfavorable case we can take a general path length distribution function in the form $P(l) = \alpha^2 l \cdot \exp(-\alpha l)$, which has a rather broad maximum (comparable with the averaged path length) at $l = \alpha^{-1}$ where $\alpha$ is a parameter. The averaged photon path length for this distribution function calculated from Eq. (10) is expressed as $\langle L\rangle = 2/(\alpha + \mu_a^0)$. We can easily obtain from (13) the following very simple criterion for applicability of the linear approximation with this path length distribution function:

$$\tfrac{1}{4}(\Delta\mu_a \cdot \langle L\rangle) \ll 1. \tag{14b}$$

Analyzing this relation one can conclude that the linear approximation should work fairly well even for cases with the broad path length distribution function if the changes in attenuation are less or the order of unity. The analytical form of the criterion for applicability of the linear approximation can also be calculated for the case of distantly separated fibers when the diffusion theory is valid. Substituting the path length distribution function obtained from the diffusion approximation for the distantly separated fibers [Eq. (4)] when calculating the averaged values in relation (13) we obtain

$$\frac{\Delta\mu_a}{\mu_a^0} \ll 4 \cdot \left(1 + \frac{\delta}{d}\right). \tag{14c}$$

We observe that for this particular case the applicability of the linear approximation is also valid for high absorption coefficient variances ($\Delta\mu_a \approx \mu_a^0$) through the spectral range under investigation when $\delta \gg d$ (weak absorption limit). Thus, the linear approximation is valid for small variances of the absorption coefficient and may extend even over this range for narrow path length distribution functions.

We assume further that the main chromophore in the tissue contributing to the strongly wavelength variable absorption is hemoglobin in oxygenated and deoxygenated form, while the contribution of other absorbers can be approximated by a smooth wavelength function. Thus, the tissue absorption coefficient is modeled as

$$\mu_a(\lambda) = \mu_a^b(\lambda) + \{c_{Hb} \cdot \varepsilon_{Hb}(\lambda) + c_{HbO_2} \cdot \varepsilon_{HbO_2}(\lambda)\} \cdot \ln(10), \tag{15}$$

where $\mu_a^b(\lambda)$ is the contribution of background to the tissue absorption coefficient (melanin, etc.), $\varepsilon$ and $c$ are the extinction coefficients and concentrations, respectively, of deoxygenated (Hb) and oxygenated (HbO$_2$) hemoglobin. The background contribution should be a smooth function of wavelength. It is also possible to take into account other tissue absorbers in Eq. (15) in the way similar to hemoglobin. For example, for analysis in the NIR wavelength range (between 700 and 1100 nm) it is necessary to add in Eq. (15) the extinction coefficients of fat and water[20,37] or the bilirubin extinction for analysis of bilirubin content in skin.[31] For further analysis we will be restricted only to hemoglobin content calculation. It is acceptable for the wavelength range between 510 and 590 nm which is used for analysis. Taking into account relations (8) and (15) and approximating the background absorption and scattering contribution by a smooth (polynomial) function of wavelength we arrive at the following simple equation for attenuation:

$$
\begin{aligned}
A_{model}(\lambda) &= \ln\left(\frac{I_0}{I}\right) \\
&= c_0 + c_1 \cdot \lambda + c_2 \cdot \lambda^2 + \langle L\rangle \\
&\quad \cdot \{c_{Hb} \cdot \varepsilon_{Hb}(\lambda) + c_{HbO_2} \cdot \varepsilon_{HbO_2}(\lambda)\} \cdot \ln(10),
\end{aligned}
\tag{16}
$$

where $c_0$, $c_1$, and $c_2$ are coefficients taking into account the contributions of background absorption and the scattering as well as the constant value of $\mu_a^0\langle L\rangle$. The $c_0$ coefficient also takes into account the uncertain constant additive entering into the experimental attenuation curve [see Eq. (20) argumentation to this]. The values of these coefficients as well as the values of $\langle L\rangle c_{Hb}$ and $\langle L\rangle c_{HbO_2}$ are obtained by minimizing the difference between fitted and experimental spectra with the least square method:

$$\chi^2 = \sum_{\lambda_i = \lambda_{min}}^{\lambda_i = \lambda_{max}} [A_{model}(\lambda_i) - A_{exp}(\lambda_i)]^2 = \min, \tag{17}$$

where $\lambda_i$ are the $N$ wavelength values at which the attenuation is measured in the range between $\lambda_{min}$ and $\lambda_{max}$. The optimal wavelength range between $\lambda_{min}$ and $\lambda_{max}$ used for analysis is chosen from the following considerations. The spectra of Hb and HbO$_2$ should differ substantially in this spectral range, whereas the contribution of other tissue absorbers and the scattering are described by smooth functions of wavelength. Thus, the wider spectral range used for analysis the greater difference attained between Hb and HbO$_2$ spectral curves resulting in error decreasing. However, the wavelength dependent contributions of scattering and other tissue absorbers are more substantial in the wider spectral range resulting in error increasing. The applicability of linear approximation [Eqs. (14a)–(14c)] is also less favorable in the wide spectral range. We found out that the spectral range between 510 nm and 590 nm is the "golden mean" for most cases of blood oxygenation calculations. The parameter $c_2$ in Eq. (16) can be omitted from the fitting in such a narrow spectral range.

The blood oxygen saturation degree $SO_2$ and relative hemoglobin concentration HbT are calculated from the above determined coefficients as follows:

$$SO_2 = \frac{\langle L \rangle c_{HbO_2}}{\langle L \rangle c_{HbO_2} + \langle L \rangle c_{Hb}} = \frac{c_{HbO_2}}{c_{HbO_2} + c_{Hb}},$$

$$HbT = \langle L \rangle \cdot (c_{Hb} + c_{HbO_2}).$$
$$(18)$$

The relative hemoglobin concentration values depend on measurement geometry (through the $\langle L \rangle$ value) and so only the relative changes taken during the measurements at the same geometry are meaningful. It should also be mentioned that for *in vivo* measurements the movement of the object (change of the distance between the fiber probe and the tissue for non-contact measurements) may result in the small random changes in $\langle L \rangle$ and, consequently, the errors in relative hemoglobin concentration monitoring, while the oxygen saturation value is less receptive to these changes.

The accuracy of the model may be estimated by the difference between fitted and experimental attenuation spectra determined by the following relation:

Error

$$= \frac{\sqrt{\chi^2/N}}{\frac{1}{N} \cdot \sum_{\lambda_i = \lambda_{min}}^{\lambda_i = \lambda_{max}} \langle L \rangle \cdot \{c_{Hb} \cdot \varepsilon_{Hb}(\lambda_i) + c_{HbO_2} \cdot \varepsilon_{HbO_2}(\lambda_i)\} \cdot \ln(10)} \cdot 100\%,$$
$$(19)$$

where the $\chi^2$ is defined by Eq.(17) and $N$ is the number of points in the spectrum range between $\lambda_{min}$ and $\lambda_{max}$. When the error value is over 50% the $SO_2$ and HbT calculation results should be considered as invalid. It may take place when the blood content is very low in the tissue so that its contribution to the absorption is compared to that of noise. It may also take place in the presence of other tissue absorbers which are not taken into account by Eq. (15) and when the influence of the scattering cannot be approximated by a smooth wavelength function in the spectral range under consideration. The discrepancy between the experiment and the model may result also from inapplicability of linear approximation (13) due to high variations of $\mu_a$ in the analyzed spectral range. The allowance for quadratic term in Eq. (8) may improve the match between experimental and fitted data in this case.

## 4  Experimental Technique

For the measurements of diffuse reflectance spectra of tissue *in vivo* and blood samples we applied a fiberoptic spectrometer LESA-5 (Biospec, Russia). An experimental setup used for *in vivo* measurements is shown in Figure 3. Light from a stabilized light source (halogen lamp) was delivered to the tissue by means of a quartz fiber. After passing through the tissue the light was collected by a receiving fiber. The output end of the receiving fiber was the input slit of the spectrometer. We applied the spectrometer with a fixed grating and a charge coupled device (CCD)-type detector. The total spectrum range (between 400 and 1000 nm) can be acquired for 0.1 s. The spectrometer was controlled by a personal com-
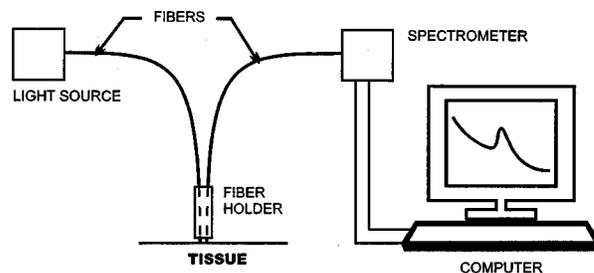


**Fig. 3** Experimental setup for measurements of diffuse reflectance spectra *in vivo*.

puter. A special program operating in the MS Windows environment allows one to acquire and display the spectra and calculate the oxygen hemoglobin saturation and the relative hemoglobin concentration in real time using the above described algorithm. For calculation we exploited only a part of the spectral range between 510 and 590 nm acquired by the spectrometer.

For *in vivo* measurements we used a fiber configuration shown in Figure 2. The distance $d$ between delivery and receiving fibers with core diameters of 200 $\mu$m and NA 0.22 was set to 2 mm. During the measurements the fibers were fixed at a distance less than half a millimeter from the tissue. This configuration allowed only diffuse reflected photons to enter into the receiving fiber. There was no contact between fibers and tissue to avoid the influence of fiber pressure on blood circulation.

To demonstrate that Taylor expansion algorithm is applicable to different geometries of the measurement resulting in different path length distribution functions, $P(l)$, of photons through a sample, we present here the results of measuring the hemoglobin oxygen saturation in blood samples during photochemical deoxygenation. The fiber configuration used for the blood samples has quite a different geometry and correspondingly another path length distribution function from that of the tissue. To prepare a blood sample some fresh blood with added heparin to avoid clotting was incubated with sulphonated aluminum phthalocyanine as photosensitizer in concentrations of 1–20 $\mu$M for 30 min. To saturate the blood with oxygen an oxygen flow passed through the blood during incubation to attain the initial hemoglobin oxygen saturation level in the range of 80%–85%. A blood drop was placed between two glasses. The glass thickness was 1.2 mm. The thickness of the blood layer was controlled with the use of a special film and was in the range of $d = 125 \pm 5$ $\mu$m. The diameter of a sample was 1.5 cm. The delivering and receiving fibers were placed at the opposite sides of a blood sample with the receiving fiber positioned at a small angle to the normal $\varphi \approx 10°$ to exclude collimated transmitted photons. Thus, in this case we actually measured the spectral diffuse transmittance of the sample. Further, these samples were irradiated with laser light at fluence rates 10–1200 mW/cm$^2$ at 670 nm incident close to normal to the glass surface. The laser irradiation was absorbed by photosensitizer present in blood and induced photochemical oxygen consumption resulting in slow decrease of the hemoglobin oxygen saturation.
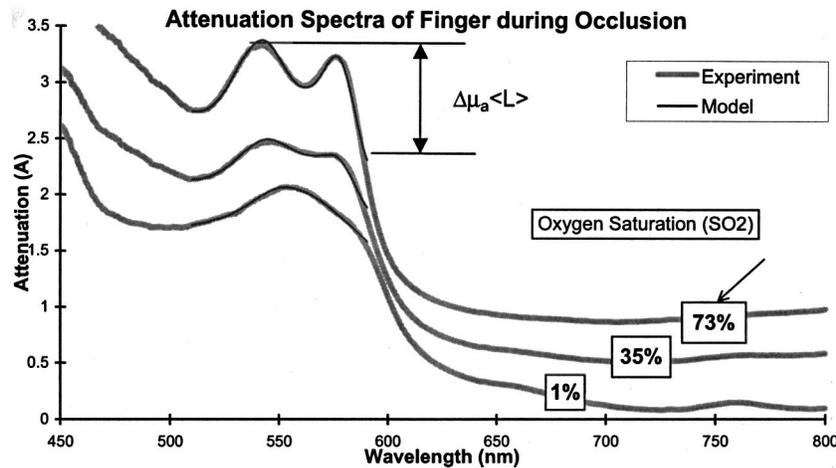
**Fig. 4** Attenuation spectra of a finger during occlusion at different times (thick gray) and fitted spectra, $A_{model}$, (thin black) in the range between 510 and 590 nm. The corresponding blood oxygen saturation $SO_2$ calculated from the model is shown in the figure.

The experimentally measured spectral dependence of the light attenuation is evaluated with the use of the following relation:

$$A_{exp}(\lambda) = \ln\left(\frac{I_{ref} - I_{dark}}{I - I_{dark}}\right), \qquad (20)$$

where $I_{ref}$ is the measured reflectance signal from the reference sample ($BaSO_4$), which has the uniform diffuse reflectance near unity in the spectral range under consideration (400–1000 nm), $I_{dark}$ is the signal in the absence of any light (dark current of CCD) and $I$ is the diffuse reflectance signal from the tissue or diffuse transmittance in the case of the blood sample. Equation (20) accounts for the spectral nonuniformity of the light source, the fiber transmission and the detector sensitivity. It should be noted that $A_{exp}(\lambda)$ as given by Eq. (20) is defined to within some constant value as compared to that of defined by Eq. (1): $A_{exp}(\lambda) = A(\lambda) + \text{const}$. This constant would be equal to zero if we can substitute the signal coming out from the delivering fiber in Eq. (20) instead of $I_{ref}$. It should be noted that $I_{ref}$ is measured with a fiber probe placed at the distance of about 1–2 cm from the reference sample surface as the $I_{ref}$ signal should approximate the wavelength dependence of photon flux coming out of the delivering fiber and wavelength dependent contribution of the scattering should be minimized. The reference signal $I_{ref}$ measured as described above differs from $I_0$ [see Eq. (1)] by some wavelength independent constant factor resulting in appearance of constant additive in the experimental attenuation curve. However, the exact value of the constant in $A_{exp}(\lambda)$ is not important for our algorithm as only its wavelength dependence matters. This additive constant is compensated by fitted $c_0$ coefficient in Eq. (16).

## 5 Results and Discussion

To demonstrate the applicability of the above described algorithm we present here the results of deoxygenation observed during the artery occlusion. The occlusion was done by tightly wrapping a rubber tape around the base of a finger, while the measurements were done on the outer surface of an upper

finger phalanx. We also did the artery occlusion by placing a pneumatic pressure cuff around an upper arm and applying pressure up to 200 mmHg (data are not shown) but found no substantial difference in deoxygenation dynamics in these two methods. Figure 4 demonstrates the attenuation spectra $A_{exp}(\lambda)$ taken from the finger of the author (A.A.S.) at different times after starting the occlusion. The spectra are shifted along the $y$ axis on arbitrary values for observation convenience, the amount of the shift is not important for calculations. We notice that the spectral line shapes strongly correlate with the blood oxygen saturation. In the range between 510 and 590 nm the modeled spectra calculated using Eq. (16) with coefficient $c_2$ responsible for quadratic contribution fixed to zero are shown in Figure 4 by black thin lines and the corresponding blood oxygen saturation values calculated from the model are given. The closeness of the experimental $A_{exp}(\lambda)$ and fitted $A_{model}(\lambda)$ spectral curves also suggests the applicability of our model in this case. For this measurement configuration the use of the spectral wavelength range between 510 and 590 nm is most suitable as the spectral features of hemoglobin are most pronounced for this range as can be seen from Figure 4. Anyway, the disadvantage of this spectral range is the small light penetration depth. The sampling depth of our measurements is the fraction of millimeter corresponding to the signal originated from skin capillary loops.[9] By close analysis of spectra shown in Figure 4 one can also notice the difference in the NIR spectral range (the appearance of a small peak at 755 nm for deoxygenated tissue) resulting from different blood oxygen saturation. However, the spectral differences here are not so pronounced, and the error in evaluation of the blood oxygen saturation in this spectral range from the above described model will be much greater. We tried to interpret the data by Taylor expansion method using the spectral range between 650 and 800 nm. As mentioned above, the deoxygenated hemoglobin has pronounced spectral feature (peak at 755 nm), but spectral dependence of the oxygenated hemoglobin is rather smooth resulting in possible cross talking between smooth background contribution, influence of the scattering [see Eq. (16)] and the contribution of the oxygenated hemoglobin. In this spectral range water con-

**Time Dependence of Oxygenation and Hemoglobine during Finger Occlusion**
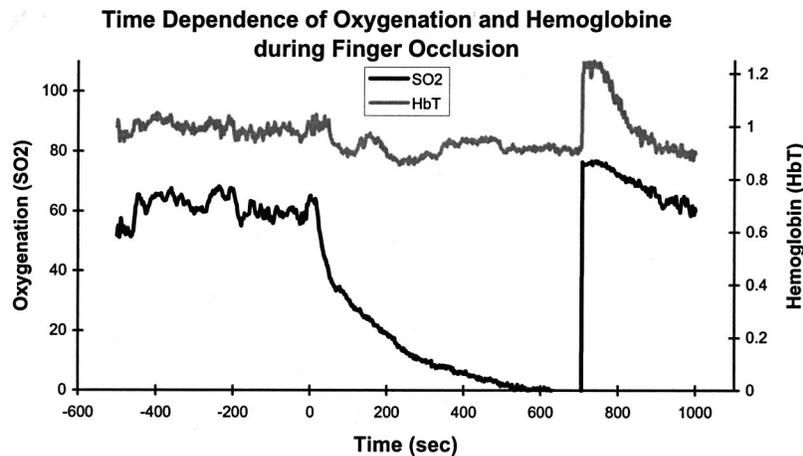


**Fig. 5** Time dependence of blood oxygen saturation ($SO_2$) and total relative hemoglobin concentration (HbT) calculated from the model during finger occlusion. The occlusion was started at $t=0$ s and released at $t=700$ s.

tribution should also be taken into account. It should be noted that the modeled attenuation curves fit fairly well into the experimental curves for the NIR range, but the blood oxygen saturation evaluated from this fitting was higher than expected. For example, before starting the occlusion $SO_2$ values calculated from NIR range alone (from 650 to 800 nm) were as high as 85%–100%. The reason for this disagreement is that the smooth contribution of the oxygenated hemoglobin in NIR may be partly compensated by a linear function of the wavelength responsible for scattering and background absorption (the above mentioned cross talking). The expansion of the spectral range to include both visible and NIR in relation (17) also resulted in an increase of the error. It is because of poor applicability of the linear approximation when the variances of the absorption coefficient are rather great [Eqs. (13) and (14)] and insufficient approximation of the background absorption and the scattering contribution by the linear function of the wavelength. One can also notice in Figure 4 the slight tendency to deviation between the experimental attenuation and the modeled curves near the interval boundary at 590 nm. If we increase the wavelength range even just to 600 nm when fitting the modeled curve by Eq. (17), this deviation would be greater. Thus, we think that with the use of the Taylor expansion method the spectral range from 510 up to 590 nm is optimal for evaluating the blood oxygen saturation and the hemoglobin relative concentration.

We can easily evaluate from Figure 4 that the measured attenuation changes $\Delta\mu_a\langle L\rangle$ in the spectral range under analysis are 0.4 and 1.0 for deoxygenated and oxygenated case, correspondingly. Substituting these values into criterion (14b) obtained for broad path length distribution function we get evidence that linear approximation is applied here though with small reserve. If we expand the analyzed spectral range even up to 650 nm, the attenuation changes would increase up to about 2.5 (see Figure 4) resulting to poor applicability of criterion (14b) in this case and giving unreasonable values for blood oxygen saturation as was mentioned above. Another estimation may be received if we assume that criterion (14c) obtained with the use of diffusion theory for distantly separated fibers is valid for our fiber probe configuration. Using the data of hemoglobin extinction spectra, one can make sure

that its variances in the absorption ($\Delta\mu_a/\mu_a^0$) in the spectral range from 510 to 590 nm are 0.4 and 0.9 for deoxygenated and oxygenated hemoglobin, correspondingly. Assuming further that averaged light penetration depth $\delta$ in this spectral range is about 1 mm, and substituting it in criterion (14c), we obtain that the linear approximation is valid for $\Delta\mu_a/\mu_a^0 \ll 6$ that is also fulfilled in our case.

Figure 5 demonstrates the monitoring of typical time behavior for the blood oxygen saturation and the relative hemoglobin concentration during the artery occlusion calculated from our model. The finger occlusion was started at $t=0$ s and released at $t=700$ s. Under normal conditions (before starting occlusion) the irregular oscillations in $SO_2$ in the range of 50%–70% are observed (time interval between $-600$ and 0 s). These oscillations are not random errors but real facts mainly due to the spatial micro nonuniformity of $SO_2$ in the skin layer and hand movements during the measurements. The value of the blood oxygen saturation in skin at rest (50%–70%) at the normal ambient temperature (20–22°C) agrees fairly well with that reported by others.[38–40] It should be noted that the measurements done at lower ambient temperatures gave the values of the blood oxygen saturation in skin at rest as low as 15%–30% (data are not shown). As may be seen from Figure 5, total hemoglobin deoxygenating in a superficial skin layer is attained 10 min after starting the occlusion. The closeness of $SO_2$ value to zero at the end of the occlusion also demonstrates the accuracy of the model. After occlusion release we observe a sharp increase for both blood oxygen saturation and relative hemoglobin concentration due to the intensive blood circulation (reactive hyperemia), which after some time are restored to their previous values. The similar results have been also observed by other researchers.[38,39] For further examples employing this algorithm for *in vivo* measurements the reader is refereed to Ref. 41.

The use of Taylor expansion algorithm for calculating oxygenation in blood samples should be more favorable than for tissues because path length distribution function for blood sample geometry is rather narrow. Really, when passing through the sample, most photons change their initial direction just slightly (single scattering) as the thickness of the

**Blood Attenuation Spectra During PDT**
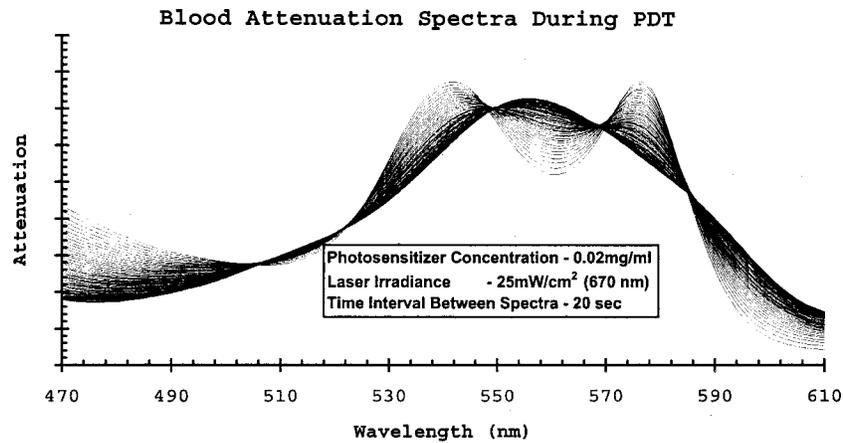


**Fig. 6** Attenuation spectra of a blood sample incubated with photosensitizer in concentration 0.02 mg/ml during photodynamic therapy with laser power density of 25 mW/cm² at 670 nm. The time interval between spectra is 20 s. The transformation of hemoglobin from oxygenated to deoxygenated form is clearly observed.

blood sample is much less than the reduced photon scattering length (inverse of reduced scattering coefficient). It means that for this configuration the photon path length distribution function has a rather sharp peak at the path length value $\langle L \rangle$ a little bit higher than the sample thickness $d$. As the angle $\varphi$ between receiving fiber and normal to the blood sample was rather small (about 10°), the broadness $\Delta L$ of path length distribution function is just about $d(\sin\varphi)^2 \approx 0.03 \cdot d$ as roughly estimated from single scattering assumption. Substituting this value of $\Delta L$ into criterion (14a) obtained for narrow path length distribution functions and evaluating the attenuation changes for blood sample $\Delta \mu_a \langle L \rangle \approx 2.5$ we can easily calculate that $\Delta \mu_a \langle L \rangle \cdot (\Delta L / \langle L \rangle)^2 \approx 0.002 \ll 1$. Thus, the criterion of applicability of linear approximation is fulfilled here with great reserve, resulting in reasonable and reliable values of blood oxygen saturation obtained in this case.

Additional reduction in noise is also achieved due to absence of subject movement during the measurements. Here we present the observation of oxygen saturation changes in a blood sample incubated with a photosensitizer under the in-

fluence of laser irradiation [photodynamic therapy (PDT)].[41–43] This model may be very useful for evaluation of oxygen consumption rate during PDT. Oxygen is consumed in photochemical reactions during PDT and steady decrease in blood oxygen saturation should be observed. The attenuation spectra taken from the blood sample during laser irradiation are shown in Figure 6. The corresponding time behavior of the blood oxygen saturation (SO₂) and the relative hemoglobin concentration (HbT) calculated with the use of the above described model are shown in Figure 7. A smooth decrease of the oxygen saturation to zero value and the constant relative hemoglobin concentration are observed. As expected, the random noise is extremely low for these measurements. We should be reminded that the fiber configurations for the tissue measurements (Figure 5) and the blood sample measurements (Figure 7) were quite different (in the second case the delivery and receiving fibers were positioned at the opposite sides of a blood sample). Nevertheless, the proposed algorithm may be successfully applied to both cases giving accurate results.
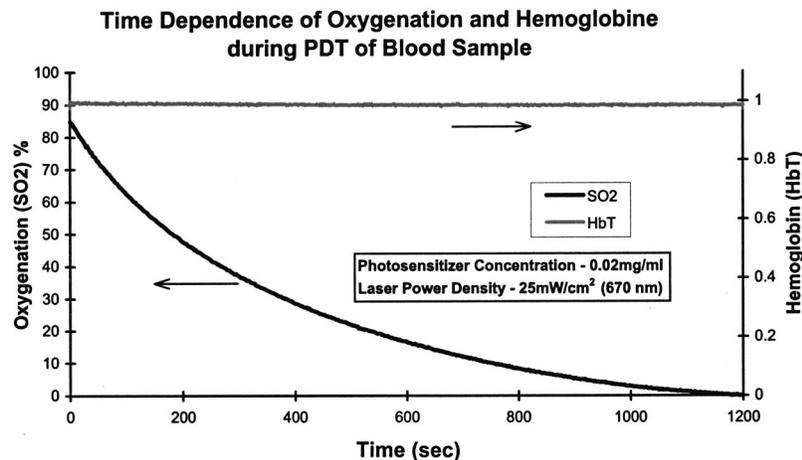


**Fig. 7** Time dependence of blood oxygen saturation (SO₂) and total relative hemoglobin concentration (HbT) in a blood sample during PDT. The values are calculated from the spectra shown in Figure 6.

# 6 Conclusion

A simple algorithm for evaluation of blood oxygen saturation and relative hemoglobin concentration was obtained here by the consistent approach of Taylor expansion of exact relation for light attenuation. The advantage of this approach is that it results in a simple, robust, not very sensitive to noise algorithm for the blood oxygen saturation, which can be implemented for calculations in real time. The algorithm may be successfully applied to the visible wavelength range for different measurement configurations as confirmed by experimental data presented in the paper. Work is in progress to apply this algorithm investigating the influence of temperatures and laser irradiation on blood oxygenation in human skin[44] and adapt this approach to the near infrared range to increase the sampling depth of the measurements.

# References

1. D. W. Lübbers and R. Wodick, "Absolute reflection photometry applied to the measurement of capillary oxyhemoglobin saturation of the skin in man," in *Oxygen Measurements in Biology and Medicine,* J. P. Payne and D. W. Hill, Eds., pp. 85–100, Butterworths, London (1975).
2. F. F. Jöbsis, "Noninvasive infrared monitoring of cerebral and myocardial oxygen sufficiency and circulatory parameters," *Science* **198**, 1264–1267 (1977).
3. N. Sato, T. Kamada, M. Shichiri, S. Kawano, H. Abe, and B. Hagihara, "Measurement of hemoperfusion and oxygen sufficiency in gastric mucosa in vivo. Evidence of mucosal hypoxia as the cause of hemorrhagic shock induced gastric mucosal lesion in rats," *Gastroenterology* **76**, 814–819 (1979).
4. G. A. Mook, A. Buursma, A. Gerding, G. Kwant, and W. G. Zijlstra, "Spectrophotometric determination of oxygen saturation of blood independent of the presence of indocyanine green," *Cardiovasc. Res.* **13**, 233–237 (1979).
5. F. W. Leung, T. Morishita, E. Livingston, T. Redy, and P. H. Guth, "Reflectance spectrophotometry for the assessment of gastroduodenal mucosal perfusion," *Am. J. Physiol.* **G52**, 797–804 (1987).
6. M. Kessler, D. K. Harrison, and J. Hoper, "Tissue oxygen measurement technique," in *Microcirculatory Technology,* C. H. Baker and W. L. Nastuk, Eds., pp. 391–425, Academic, New York (1986).
7. J. W. Feather, M. Hajiazadeh-Safar, G. Leslie, and J. B. Dawson, "A portable scanning reflectance spectrophotometer using visible wavelengths for rapid measurements of skin pigments," *Phys. Med. Biol.* **34**, 807–820 (1989).
8. V. B. Loschenov, M. I. Kuzin, V. G. Arjushenko, and V. I. Konov, "Study of tissue fluorescence spectra *in situ*," *Proc. SPIE* **1066**, 271–274 (1989).
9. K. H. Frank, M. Kessler, K. Appelbaum, and W. Dümmler, "The Erlangen micro-lightguide spectrophotometer EMPHO I," *Phys. Med. Biol.* **34**, 1883–1900 (1989).
10. E. M. Sevic, B. Chance, J. Leigh, S. Nioka, and M. Maris, "Quantitation of time- and frequency-resolved optical spectra for the determination of tissue oxygenation," *Anal. Biochem.* **195**, 330–351 (1991).
11. A. H. Hielscher, F. K. Tittel, and S. L. Jacques, "Non invasive monitoring of blood oxygenation by phase resolved transmission spectroscopy," *Proc. SPIE* **1888**, 275–288 (1993).
12. D. W. Lübbers, "Chemical in vivo monitoring by optical sensors in medicine," *Sens. Actuators B* **11**, 253–262 (1993).
13. L. V. Tanin, V. A. Lapina, S. C. Dick, S. A. Aleksandrov, and R. M. Tanina, "Spectral two-wavelength method of quantitative estimation of oxyhemoglobin concentration in the human skin blood flow in vivo," *Proc. SPIE* **1887**, 158–164 (1993).
14. R. Graaf, "Tissue optics applied to reflectance pulse oximetry," PhD thesis, University of Groningen (1993).
15. S. J. Matcher and C. E. Cooper, "Absolute quantification of deoxy-hemoglobin concentration in tissue by near infrared spectroscopy," *Phys. Med. Biol.* **39**, 1295–1312 (1994).
16. N. M. Kuzin, V. B. Loschenov, A. A. Stratonnikov, O. V. Artemjeva, V. V. Levkin, and S. S. Kharnas, "Method of oxygenation saturation evaluation of stomach mucous after subtotal cancer resection," *Proc. SPIE* **2328**, 98–101 (1994).
17. H. Liu, D. A. Boas, Y. Zhang, A. G. Yodh, and B. Chance, "A simplified approach to characterize optical properties and blood oxygenation in tissue using continuous near infrared light," *Proc. SPIE* **2389**, 496–502 (1995).
18. S. J. Matcher, C. E. Elwell, C.E. Cooper, M. Cope, and D. T. Delpy, "Performance comparison of several published tissue near-infrared spectroscopy algorithms," *Anal. Biochem.* **227**, 54–67 (1995).
19. E. L. Hull and T. H. Foster, "Noninvasive near-infrared hemoglobin spectroscopy for in vivo monitoring of tumor oxygenation and response to oxygen modifiers," *Proc. SPIE* **2927**, 355–364 (1997).
20. M. A. Franceschini, S. Fantini, A. Cerussi, B. Barbieri, B. Chance, and E. Gratton, "Quantitative spectroscopic determination of hemoglobin concentration and saturation in a turbid medium. Analysis of the effect of water absorption," *J. Biomed. Opt.* **2**, 147–153 (1997).
21. T. Shiga, K. Yamamoto, K. Tanabe, Y. Nakase, and B. Chance, "Study of an algorithm based on model experiments and diffusion theory for portable tissue oximeter," *J. Biomed. Opt.* **2**, 154–161 (1997).
22. M. H. Smith, K. R. Denninghoff, L. W. Hillman, and R. A. Chipman, "Oxygen saturation measurements of blood in retinal vessels during blood loss," *J. Biomed. Opt.* **3**, 296–303 (1998).
23. W. G. Zijlstra, A. Buursma, and W. P. Meeuwsen-van der Roest, "Absorption spectra of human fetal and adult oxyhemoglobin, deoxyhemoglobin, carboxyhemoglobin and methhemoglobin," *Clin. Chem.* **37**, 1633–1638 (1991).
24. M. S. Patterson, B. Chance, and B. C. Wilson, "Time resolved reflectance and transmittance for the noninvasive measurements of tissue optical properties," *Appl. Opt.* **28**, 2331–2336 (1989).
25. A. Kienle and M. S. Patterson, "Improved solutions of the steady-state and the time-resolved diffusion equations for reflectance from semi-infinite turbid medium," *J. Opt. Soc. Am.* **14**, 246–254 (1997).
26. T. J. Farrell, M. S. Patterson, and B. Wilson, "A diffusion theory model of spatially resolved, steady-state diffuse reflectance for the noninvasive determination of tissue optical properties in vivo, " *Med. Phys.* **19**, 879–888 (1992).
27. A. Kienle, L. Lilge, M. S. Patterson, R. Hibst, R. Steiner, and B. C. Wilson, "Spatially resolved diffuse reflectance measurements for noninvasive determination of the optical scattering and absorption coefficients of biological tissue," *Appl. Opt.* **35**, 2304–2313 (1995).
28. R. Bays, G. Wagnieres, D. Robert, D. Braichotte, J. F. Savary, P. Monnier, and H. Van den Berg, "Clinical determination of tissue optical properties by endoscopic spatially resolved reflectometry," *Appl. Opt.* **35**, 1756–1765 (1996).
29. F. Bevilacqua, D. Piguet, P. Marquet, J. D. Gross, B. J. Tromberg, and C. Depeursinge, "In vivo local determination of tissue optical properties," *Proc. SPIE* **3194**, 262–268 (1997).
30. J. S. Dam, P. E. Andersen, T. Dalgaard, and P. E. Fabricius, "Determination of tissue optical properties from diffuse reflectance profiles by multivariate calibration," *Appl. Opt.* **37**, 772–778 (1998).
31. S. Jacques, I. Saidi, A. Ladner, and D. Oelberg, "Developing an optical fiber reflectance spectrometer to monitor bilirubinemia in neonates," *Proc. SPIE* **2975**, 115–124 (1997).
32. J. Liang, S. V. Huffel, and P. Casaer, "Principal component and canonical correlation analysis of near infrared spectra," *Proc. SPIE* **2389**, 660–668 (1995).
33. W. Cui, C. Kumar, and B. Chance, "Experimental study of migration depth for the photons measured at sample surface," *Proc. SPIE* **1431**, 180–189 (1989).
34. S. Feng, F. Zeng, and B. Chance, "Monte Carlo simulations of photon migration path distributions in multiple scattering media," *Proc. SPIE* **1888**, 78–97 (1993).
35. R. C. Haskell, L. O. Svaasand, T. T. Tsay, T. C. Feng, M. McAdams, and B. J. Tromberg, "Boundary conditions for the diffusion equation in radiative transfer," *J. Opt. Soc. Am. A* **11**, 2727–2741 (1994).
36. R. Graaff, J. G. Aarnoudse, J. R. Zijp, P. M. A. Sloot, F. F. M. de Mul, J. Greve, and M. H. Koelnik, "Reduced light-scattering properties for

mixtures of spherical particles: A simple approximation derived from Mie calculations,'' *Appl. Opt.* **31**, 1370–1376 (1992).

37. H. Heusmann, J. Kölzer, R. Puls, J. Otto, S. Heywang-Köbrunner, and W. Zinh, ''Spectral transillumination of human breast tissue,'' *Proc. SPIE* **2389**, 798–808 (1995).

38. D. K. Harrison, S. D. Evans, N. C. Abbot, J. Swanson Beck, and P. T. McCollumn, ''Spectrophotometric measurements of haemoglobin saturation and concentration in skin during the turberculin reaction in normal human subjects,'' *Clin. Phys. Physiol. Meas.* **13**(4), 349–363 (1992).

39. D. J. Wallace, B. Michener, D. Choudhary, M. Levi, P. Fennelly, D. M. Hueber, and B. Barbieri, ''Summary of the results of a 95 subject human clinical trial for the diagnosis of peripheral vascular disease using a near infrared frequency domain hemoglobin spectrometer,'' *Proc. SPIE* **3597**, 300–316 (1999).

40. M. Oda, Y. Yamashita, T. Nakano, A. Suzuki, K. Shimizu, I. Hirano, F. Shimomura, E. Ohmae, T. Suzuki, and Y. Tsuchiya, ''Near infrared time-resolved spectroscopy system for tissue oxygenation monitor,'' *Proc. SPIE* **3597**, 611–617 (1999).

41. A. A. Stratonnikov, A. Y. Douplik, and V. B. Loschenov, ''Oxygen consumption and its transport in tissues during photodynamic therapy of tumors and whole blood,'' in *Oxygen Transport to Tissues XXI,* A. Eke and D. T. Delpy, Eds., pp. 515–524, Kluwer/Plenum, New York (1999).

42. A. Y. Douplik, A. A. Stratonnikov, V. B. Loschenov, V. S. Lebedeva, V. M. Derkacheva, A. Vitkin, V. D. Rumyanceva, S. G. Kuzmin, A. F. Mironov, and E. A. Luk'Yanets, ''The study of photodynamic reactions in human blood,'' *J. Biomed. Opt.* **5**(3), 338–349 (2000).

43. A. A. Stratonnikov, A. Yu. Douplik, and V. B. Loschenov, ''Mathematical model of oxygen consumption and photobleaching in blood incubated with photosensitizer during light irradiation,'' *Photochem. Photobiol.* (2001) (in press).

44. A. A. Stratonnikov, N. V. Ermishova, and V. B. Loschenov, ''Influence of red laser irradiation on hemoglobin oxygen saturation and blood volume in human skin *in vivo*,'' *Proc. SPIE* **4257**, 57–64 (2001).